MOHeaCAN

Estimating the global Ocean Heat Content and the Earth Energy Imbalance products from space

Algorithm Theoretical Basis Document

	Name	Organisation	Date	Visa
Written by:	Victor Rousseau Michaël Ablain Florence Marti Robin Fraudeau	Magellium	24/04/2023	
	Benoit Meyssignac Alejandro Blazquez	LEGOS		
Checked by:	Michaël Ablain	Magellium	24/04/2023	
Approved by:	Joël Dorandeu	Magellium	24/04/2023	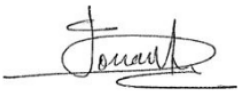

Document reference:	GIECCO-DT-067-MAG_ATBD
Edition.Revision:	1.8
Date Issued:	24/04/2023
Data Set Version:	v5-0 (date of release: April-2023)

Document evolution sheet

Ed.	Rev.	Date	Purpose evolution	Comments
1	0	02/03/2019	Creation of document	
1	1	09/09/2020		Feedback from MTR
1	2	13/10/2020	Release of first product version (v1-0)	Consideration of observations and requests from ESA's first review Integration of a regional grid of GIA in altimetry data Update of the comments/limitations
1	3	26/04/2021	Release of new product version (v2-0)	Use of a new manometric sea level solutions ensemble.
1	4	09/09/2021	Release of new product version (v2-1)	Addition of the elastic correction for the recent melting and contributions from other climate reservoirs to EEI (β coefficient).
1	5	08/12/2021	Release of new product version (v3-0)	Add gap filling algorithm on manometric sea level data Use of a new manometric sea level solutions ensemble (V1.5) Use of new C3S altimetry data version (vDT2021) New format of OHC-EEI netCDF file (splitted in 2 different files) New method for compute temporal derivative of GOHC
1	6	30/06/2022	Release of new product version (v4-0)	Use of a new manometric sea level solutions ensemble (V1.5.1) Correction on altimetry data (wet tropospheric correction data on Jason-3 observations) Use of a time varying IEEH New method for computing EEI from regional OHC grids
1	7	07/10/2022	Minor corrections	Update of the introduction section 2 and sections 2.1, 3.4.2, 4.5.5
1	8	24/04/2023	Release of new product version (v5-0)	Rename of Ocean Mass change to Manometric sea level change Use of new GMSL error budget from Guerou et al 2022 (section 5.2)

				Use of new manometric component of the sea level solutions ensemble (section 3.2) Use of a time-constant IEEH estimated with the ECCOr4v4 model (section 3.4) Update estimation of other reservoir contribution to the EEI (section 4.5.8.2)

Contents

List of figures

List of tables

1. Introduction

1.1. Executive summary

Since the industrial era, anthropogenic emissions of greenhouse gases (GHG) in the atmosphere have lowered the total amount of infrared energy radiated by the Earth towards space. Now the Earth is emitting less energy towards space than it receives radiative energy from the sun. As a consequence there is an energy imbalance (EEI) at the top of the Atmosphere (Hansen et al., 2011; Trenberth et al., 2014). It is essential to estimate and analyse the Earth Energy Imbalance (EEI) if we want to understand the Earth's changing climate. Measuring the EEI is challenging because the EEI is a globally integrated variable whose variations are small (of the order of several tenth of $W.m^{-2}$, von Schuckmann et al. (2016) compared to the amount of energy entering and leaving the climate system (of ~340 $W.m^{-2}$, L'Ecuyer et al., 2015). An accuracy of <0.3 $W.m^{-2}$ at decadal time scales is necessary to evaluate the long term mean EEI associated with anthropogenic forcing. Ideally an accuracy of <0.1 $W.m^{-2}$ at decadal time scales is desirable if we want to monitor future changes in EEI which shall be non-controversial science based information used by the GHG mitigation policies (Meyssignac et al., 2019).

EEI can be estimated by an inventory of heat changes in the different reservoirs - the atmosphere, the land, the cryosphere and the ocean. As the ocean concentrates the vast majority of the excess of energy (~91%) in the form of heat (IPCC, Forster et al., 2021), the global Ocean Heat Content (OHC) places a strong constraint on the EEI estimate.

In the MOHeaCAN project, the OHC is estimated from the measurement of the thermal expansion of the ocean based on differences between the total sea-level content derived from altimetry measurements and the manometric sea level derived from gravimetry data (noted space geodetic or "Altimetry-Gravimetry" approach). This space geodetic approach provides consistent spatial and temporal sampling of the ocean during GRACE(-FO) era, it samples nearly the entire global oceans, except for polar regions, and it provides estimates of the OHC over the ocean's entire depth. An extension is also realized prior to the GRACE(-FO) era with the use of the estimation of the global mass content from the ESA'S CCI Sea Level Budget Closure (SLBC_cci). It complements the OHC estimation from Argo (direct measurement of in situ temperature based on temperature/salinity profiles).

MOHeaCAN project's objectives were to develop novel algorithms, estimate realistic OHC uncertainties thanks to a rigorous error budget of the altimetric and gravimetric instruments, in order to reach the challenging target for the uncertainty quantification of 0.3 $W. m^{-2}$ which then allow our estimate to contribute to better understand the Earth's climate system.

1.2. Scope and objectives

This document is the Algorithm Theoretical Basis Document (ATBD) of the MOHeaCAN product initially supported by ESA and now supported by CNES. This ATBD is dedicated to the description and justification of the algorithms used in the generation of the **OHC and EEI product**. A scientific validation of the OHC-EEI MOHeaCAN product (v2-1) is described in Marti et al. (2022).

The calculation of OHC and EEI product is divided in several steps as presented in Figure 1. The first step is to process the input data from the altimetry and spatial gravimetry measurements to allow their differences to be calculated in the next step. Then the processing of the OHC at the regional level can thus be carried out. The EEI is obtained from the global Ocean Heat Uptake (GOHU) which is derived from the global OHC. The last step consists in computing uncertainties of OHC and EEI product, propagating the errors from input data until the final product. This stage is performed on OHC and EEI resulting from the computation at global level only.

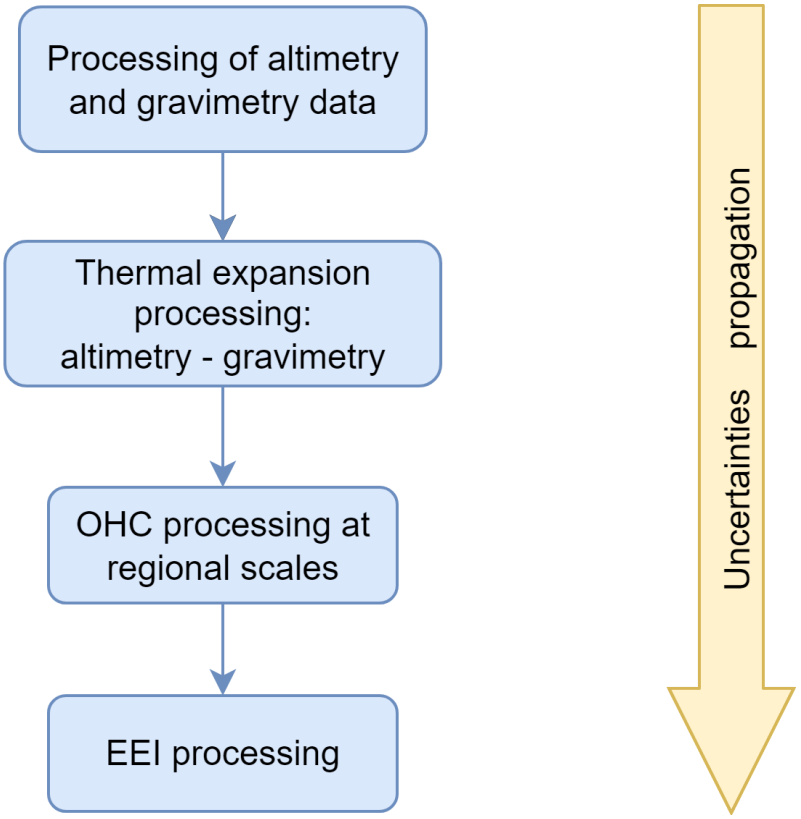

Figure 1: MOHeaCAN processing chain steps for the estimation of OHC and EEI and its uncertainties

This ATBD is divided into 4 sections. We first give a brief summary of the method and describe the physical principle of the space geodetic approach. We then present the input data for the processing chain, mainly altimetry, gravimetry and in-situ observations. Finally we explain how the OHC change is calculated at spatial regional scale before presenting the uncertainty propagation methodology in the last section.

1.3. Document structure

In addition to this introduction, the document is organised as follows:

- Section 2 explains the physical principle of the space geodetic approach and OHC change calculation.
- Section 3 presents the input data of the MOHeaCAN processing chain.
- Section 4 provides a detailed description and justification of every step in the OHC and EEI computation.
- Section 5 provides a detailed description and justification of the uncertainty propagation methodology until the final OHC-EEI product.

1.4. Applicable documents

Id.	Ref.	Description
AD1	GIECCO-DT-068-MAG_PUM	Product user manual (PUM)

Table 1: List of applicable documents

1.5. Reference documents

Id.	Ref.	Description
RD1	-	C3S data store: https://cds.climate.copernicus.eu/
RD2	D3.SL.1-v2.0_PUGS_of_v2DT2021_SeaLevel_products_v1.1_APPROVED_Ver1.pdf	Product user manual of sea level daily gridded data for the global ocean from 1993 to present from Copernicus Climate Change Service (C3S): https://datastore.copernicus-climate.eu/documents/satellite-sea-level/vDT2021/D3.SL.1-v2.0_PUGS_of_v2DT2021_SeaLevel_products_v1.1_APPROVED_Ver1.pdf
RD3	D1.SL.2-v2.0_ATBD_of_v2DT2021_SeaLevel_products_v1.1_APPROVED_Ver1.pdf	Algorithm Theoretical Basis Document of sea level daily gridded data for the global ocean from 1993 to present from Copernicus Climate Change Service (C3S): : https://datastore.copernicus-climate.eu/documents/satellite-sea-level/vDT2021/D1.SL.2-v2.0_ATBD_of_v2DT2021_SeaLevel_products_v1.1_APPROVED_Ver1.pdf
RD4	ftp://ftp.legos.obs-mip.fr/pub/soa/gravimetrie/grace_legos/	Update of the ensemble of the manometric sea level solutions provided by Blazquez et al. (2018) on LEGOS FTP site.

RD5	https://grace.jpl.nasa.gov/data/data-updates/	Jet Propulsion Laboratory (NASA) website dedicated to Gravity recovery and climate experiment, GRACE and GRACE-FO missions.
RD6	https://www.ecco-group.org/products-ECCO-V4r4.htm	Ecco groupe website dedicated to ECCO-V4r4 reanalysis product access
RD7	https://catalogue.ceda.ac.uk/uuid/17c2ce31784048de93996275ee976fff	CEDA Archive for ESA Sea Level Budget Closure Climate Change Initiative (SLBC_cci) dataset

Table 2: List of reference documents

1.6. Bibliography

- Ablain, M., Cazenave, A., Larnicol, G., Balmaseda, M., Cipollini, P., Faugère, Y., Fernandes, M. J., Henry, O., Johannessen, J. A., Knudsen, P., Andersen, O., Legeais, J., Meyssignac, B., Picot, N., Roca, M., Rudenko, S., Scharffenberg, M. G., Stammer, D., Timms, G., and Benveniste, J.: Improved sea level record over the satellite altimetry era (1993–2010) from the Climate Change Initiative project, Ocean Sci., 11, 67–82, https://doi.org/10.5194/os-11-67-2015, 2015.
- Ablain, M., Jugier, R., Zawadki, L., Taburet, N., Cazenave, A., and Meyssignac, B.: The TOPEX-A Drift and Impacts on GMSL Time Series, AVISO Website, October 2017, 2017.
- Ablain, M., Meyssignac, B., Zawadzki, L., Jugier, R., Ribes, A., Cazenave, A., and Picot, N.: Error variance-covariance matrix of global mean sea level estimated from satellite altimetry (TOPEX, Jason 1, Jason 2, Jason 3), https://doi.org/10.17882/58344, 2018.
- Ablain, M., Meyssignac, B., Zawadzki, L., Jugier, R., Ribes, A., Spada, G., Benveniste, J., Cazenave, A., and Picot, N.: Uncertainty in satellite estimates of global mean sea-level changes, trend and acceleration, Earth Syst. Sci. Data, 11, 1189–1202, https://doi.org/10.5194/essd-11-1189-2019, 2019.
- Barnoud, A., Pfeffer, J., Guérou, A., Frery, M.-L., Siméon, M., Cazenave, A., Chen, J., Llovel, W., Thierry, V., Legeais, J.-F., and Ablain, M.: Contributions of altimetry and Argo to non-closure of the global mean sea level budget since 2016, Geophys. Res. Lett., https://doi.org/10.1029/2021gl092824, 2021.
- Barnoud, A., Picard, B., Meyssignac, B., Marti, F., Ablain, M., and Roca, R.: Reducing the Uncertainty in the Satellite Altimetry Estimates of Global Mean Sea Level Trends Using Highly Stable Water Vapor Climate Data Records, J. Geophys. Res. Oceans, 128, e2022JC019378, https://doi.org/10.1029/2022JC019378, 2023a.
- Barnoud, A., Pfeffer, J., Cazenave, A., Fraudeau, R., Rousseau, V., and Ablain, M.: Revisiting the global mean ocean mass budget over 2005–2020, Ocean Sci., 19, 321–334, https://doi.org/10.5194/os-19-321-2023, 2023b.
- Blazquez, A., Meyssignac, B., Lemoine, J., Berthier, E., Ribes, A., and Cazenave, A.: Exploring the uncertainty in GRACE estimates of the mass redistributions at the Earth surface: implications for the global water and sea level budgets, Geophys. J. Int., 215, 415–430, https://doi.org/10.1093/gji/ggy293, 2018.
- Carrère, L. and Lyard, F.: Modeling the barotropic response of the global ocean to atmospheric wind and pressure forcing - comparisons with observations, Geophys. Res. Lett., 30, 1275, https://doi.org/10.1029/2002GL016473, 2003.

- Church, J. A., White, N. J., Konikow, L. F., Domingues, C. M., Cogley, J. G., Rignot, E., Gregory, J. M., Broeke, M. R. van den, Monaghan, A. J., and Velicogna, I.: Revisiting the Earth's sea-level and energy budgets from 1961 to 2008, Geophys. Res. Lett., 38, https://doi.org/10.1029/2011GL048794, 2011.
- Dieng, H. B., Cazenave, A., Meyssignac, B., and Ablain, M.: New estimate of the current rate of sea level rise from a sea level budget approach, Geophys. Res. Lett., 44, 3744–3751, https://doi.org/10.1002/2017gl073308, 2017.
- ECCO Consortium, Fukumori, I., Wang, O., Fenty, I., Forget, G., Heimbach, P., and Ponte, R. M.: Synopsis of the ECCO central production global ocean and sea-ice state estimate (version 4 release 4), Zenodo, 2020.
- Forget, G., Campin, J.-M., Heimbach, P., Hill, C., Ponte, R., and Wunsch, C.: ECCO version 4: An integrated framework for non-linear inverse modeling and global ocean state estimation, Geosci. Model Dev., 8, 3071–3104, 2015.
- Forster, P., Storelvmo, T., Armour, K., Collins, W., Dufresne, J.-L., Frame, D., Lunt, D., Mauritsen, T., Palmer, M., and Watanabe, M.: The Earth's energy budget, climate feedbacks, and climate sensitivity, 2021.
- Frederikse, T., Riva, R. E. M., and King, M. A.: Ocean Bottom Deformation Due To Present-Day Mass Redistribution and Its Impact on Sea Level Observations, Geophys. Res. Lett., 44, 12,306-12,314, https://doi.org/10.1002/2017GL075419, 2017.
- Gregory, J. M. and Lowe, J. A.: Predictions of global and regional sea-level rise using AOGCMs with and without flux adjustment, Geophys. Res. Lett., 27, 3069–3072, https://doi.org/10.1029/1999GL011228, 2000.
- Gregory, J. M., Griffies, S. M., Hughes, C. W., Lowe, J. A., Church, J. A., Fukimori, I., Gomez, N., Kopp, R. E., Landerer, F., Cozannet, G. L., Ponte, R. M., Stammer, D., Tamisiea, M. E., and van de Wal, R. S. W.: Concepts and Terminology for Sea Level: Mean, Variability and Change, Both Local and Global, Surv. Geophys., 40, 1251–1289, https://doi.org/10.1007/s10712-019-09525-z, 2019.
- Guérou, A., Meyssignac, B., Prandi, P., Ablain, M., Ribes, A., and Bignalet-Cazalet, F.: Current observed global mean sea level rise and acceleration estimated from satellite altimetry and the associated uncertainty, All Depths/Remote Sensing/All Geographic Regions/Sea level/Oceans and climate, https://doi.org/10.5194/egusphere-2022-330, 2022.
- Hansen, J., Sato, M., Kharecha, P., and von Schuckmann, K.: Earth's energy imbalance and implications, Atmospheric Chem. Phys., 11, 13421–13449, https://doi.org/10.5194/acp-11-13421-2011, 2011.
- Horwath, M., Gutknecht, B. D., Cazenave, A., Palanisamy, H. K., Marti, F., Marzeion, B., Paul, F., Bris, R. L., Hogg, A. E., Otosaka, I., Shepherd, A., Döll, P., Cáceres, D., Schmied, H. M., Johannessen, J. A., Nilsen, J. E. Ø., Raj, R. P., Forsberg, R., Sørensen, L. S., Barletta, V. R., Simonsen, S. B., Knudsen, P., Andersen, O. B., Randall, H., Rose, S. K., Merchant, C. J., Macintosh, C. R., Schuckmann, K. von, Novotny, K., Groh, A., Restano, M., and Benveniste, J.: Global sea-level budget and ocean-mass budget, with focus on advanced data products and uncertainty characterisation, Earth Syst. Sci. Data, 14, 411–447, https://doi.org/10.5194/essd-14-411-2022, 2022.
- Kuhlbrodt, T. and Gregory, J. M.: Ocean heat uptake and its consequences for the magnitude of sea level rise and climate change, Geophys. Res. Lett., 39, https://doi.org/10.1029/2012GL052952, 2012.
- L'Ecuyer, T. S., Beaudoing, H. K., Rodell, M., Olson, W., Lin, B., Kato, S., Clayson, C. A., Wood, E., Sheffield, J., Adler, R., Huffman, G., Bosilovich, M., Gu, G., Robertson, F., Houser, P. R., Chambers, D., Famiglietti, J. S., Fetzer, E., Liu, W. T., Gao, X., Schlosser, C. A., Clark, E., Lettenmaier, D. P., and Hilburn, K.: The Observed State of the Energy Budget in the Early Twenty-First Century, J. Clim., 28, 8319–8346,

https://doi.org/10.1175/JCLI-D-14-00556.1, 2015.
- Legeais, J.-F., Meyssignac, B., Faugère, Y., Guerou, A., Ablain, M., Pujol, M.-I., Dufau, C., and Dibarboure, G.: Copernicus Sea Level Space Observations: A Basis for Assessing Mitigation and Developing Adaptation Strategies to Sea Level Rise, Front. Mar. Sci., 8, 2021.
- Processing of SLR Observations at CNES.: http://www.egsiem.eu/images/Newsletters/EGSIEM_newsletter_no10.pdf, last access: 31 August 2020.
- Levitus, S., Antonov, J. I., Boyer, T. P., Baranova, O. K., Garcia, H. E., Locarnini, R. A., Mishonov, A. V., Reagan, J. R., Seidov, D., Yarosh, E. S., and Zweng, M. M.: World ocean heat content and thermosteric sea level change (0–2000 m), 1955–2010, Geophys. Res. Lett., 39, https://doi.org/10.1029/2012GL051106, 2012.
- Llovel, W., Purkey, S., Meyssignac, B., Blazquez, A., Kolodziejczyk, N., and Bamber, J.: Global ocean freshening, ocean mass increase and global mean sea level rise over 2005–2015, Sci. Rep., 9, 17717, https://doi.org/10.1038/s41598-019-54239-2, 2019.
- Loeb, N. G., Doelling, D. R., Wang, H., Su, W., Nguyen, C., Corbett, J. G., Liang, L., Mitrescu, C., Rose, F. G., and Kato, S.: Clouds and the Earth's Radiant Energy System (CERES) Energy Balanced and Filled (EBAF) Top-of-Atmosphere (TOA) Edition-4.0 Data Product, J. Clim., 31, 895–918, https://doi.org/10.1175/JCLI-D-17-0208.1, 2018.
- Marti, F., Blazquez, A., Meyssignac, B., Ablain, M., Barnoud, A., Fraudeau, R., Jugier, R., Chenal, J., Larnicol, G., Pfeffer, J., Restano, M., and Benveniste, J.: Monitoring the ocean heat content change and the Earth energy imbalance from space altimetry and space gravimetry, Earth Syst. Sci. Data, 14, 229–249, https://doi.org/10.5194/essd-14-229-2022, 2022a.
- Marti, F., Blazquez, A., Meyssignac, B., Ablain, M., Barnoud, A., Fraudeau, R., Jugier, R., Chenal, J., Larnicol, G., Pfeffer, J., Restano, M., and Benveniste, J.: Monitoring the ocean heat content change and the Earth energy imbalance from space altimetry and space gravimetry, Earth Syst. Sci. Data, https://doi.org/10.5194/essd-2021-220, 2022b.
- Meyssignac, B., Boyer, T., Zhao, Z., Hakuba, M. Z., Landerer, F. W., Stammer, D., Köhl, A., Kato, S., L'Ecuyer, T., Ablain, M., Abraham, J. P., Blazquez, A., Cazenave, A., Church, J. A., Cowley, R., Cheng, L., Domingues, C. M., Giglio, D., Gouretski, V., Ishii, M., Johnson, G. C., Killick, R. E., Legler, D., Llovel, W., Lyman, J., Palmer, M. D., Piotrowicz, S., Purkey, S. G., Roemmich, D., Roca, R., Savita, A., Schuckmann, K. von, Speich, S., Stephens, G., Wang, G., Wijffels, S. E., and Zilberman, N.: Measuring Global Ocean Heat Content to Estimate the Earth Energy Imbalance, Front. Mar. Sci., 6, https://doi.org/10.3389/fmars.2019.00432, 2019.
- Piecuch, C. G. and Ponte, R. M.: Mechanisms of interannual steric sea level variability, Geophys. Res. Lett., 38, https://doi.org/10.1029/2011GL048440, 2011.
- Piecuch, C. G., Quinn, K. J., and Ponte, R. M.: Satellite-derived interannual ocean bottom pressure variability and its relation to sea level, Geophys. Res. Lett., 40, 3106–3110, https://doi.org/10.1002/grl.50549, 2013.
- Prandi, P., Meyssignac, B., Ablain, M., Spada, G., Ribes, A., and Benveniste, J.: Local sea level trends, accelerations and uncertainties over 1993–2019, Sci. Data, 8, 1, https://doi.org/10.1038/s41597-020-00786-7, 2021.
- Russell, G. L., Gornitz, V., and Miller, J. R.: Regional sea level changes projected by the NASA/GISS Atmosphere-Ocean Model, Clim. Dyn., 16, 789–797, https://doi.org/10.1007/s003820000090, 2000.
- von Schuckmann, K., Palmer, M. D., Trenberth, K. E., Cazenave, A., Chambers, D., Champollion, N., Hansen, J., Josey, S. A., Loeb, N., Mathieu, P.-P., Meyssignac, B., and Wild, M.: An imperative to monitor Earth's energy imbalance, Nat. Clim. Change, 6, 138, 2016.

- Spada, G. and Melini, D.: On Some Properties of the Glacial Isostatic Adjustment Fingerprints, Water, 11, 1844, https://doi.org/10.3390/w11091844, 2019.
- Sun, Y., Riva, R., and Ditmar, P.: Optimizing estimates of annual variations and trends in geocenter motion and J2 from a combination of GRACE data and geophysical models, J. Geophys. Res. Solid Earth, 121, 8352–8370, https://doi.org/10.1002/2016JB013073, 2016.
- Tang, L., Li, J., Chen, J., Wang, S.-Y., Wang, R., and Hu, X.: Seismic Impact of Large Earthquakes on Estimating Global Mean Ocean Mass Change from GRACE, Remote Sens., 12, 935, https://doi.org/10.3390/rs12060935, 2020.
- Taylor, J. R.: An Introduction to Error Analysis: The Study of Uncertainties in Physical Measurements, 2nd ed., University Science Books, Sausalito, California, 344 pp., 1997.
- Trenberth, K. E., Fasullo, J. T., and Balmaseda, M. A.: Earth's Energy Imbalance, J. Clim., 27, 3129–3144, https://doi.org/10.1175/JCLI-D-13-00294.1, 2014.
- Wahr, J., Swenson, S., Zlotnicki, V., and Velicogna, I.: Time-variable gravity from GRACE: First results: TIME-VARIABLE GRAVITY FROM GRACE, Geophys. Res. Lett., 31, n/a-n/a, https://doi.org/10.1029/2004GL019779, 2004.
- Watson, C. S., White, N. J., Church, J. A., King, M. A., Burgette, R. J., and Legresy, B.: Unabated global mean sea-level rise over the satellite altimeter era, Nat. Clim. Change, 5, 565–568, https://doi.org/10.1038/nclimate2635, 2015.
- WCRP Global Sea Level Budget Group: Global sea-level budget 1993–present, Earth Syst. Sci. Data, 10, 1551–1590, https://doi.org/10.5194/essd-10-1551-2018, 2018.
- Wong, A. P. S., Wijffels, S. E., Riser, S. C., Pouliquen, S., Hosoda, S., Roemmich, D., Gilson, J., Johnson, G. C., Martini, K., Murphy, D. J., Scanderbeg, M., Bhaskar, T. V. S. U., Buck, J. J. H., Merceur, F., Carval, T., Maze, G., Cabanes, C., André, X., Poffa, N., Yashayaev, I., Barker, P. M., Guinehut, S., Belbéoch, M., Ignaszewski, M., Baringer, M. O., Schmid, C., Lyman, J. M., McTaggart, K. E., Purkey, S. G., Zilberman, N., Alkire, M. B., Swift, D., Owens, W. B., Jayne, S. R., Hersh, C., Robbins, P., West-Mack, D., Bahr, F., Yoshida, S., Sutton, P. J. H., Cancouët, R., Coatanoan, C., Dobbler, D., Juan, A. G., Gourrion, J., Kolodziejczyk, N., Bernard, V., Bourlès, B., Claustre, H., D'Ortenzio, F., Le Reste, S., Le Traon, P.-Y., Rannou, J.-P., Saout-Grit, C., Speich, S., Thierry, V., Verbrugge, N., Angel-Benavides, I. M., Klein, B., Notarstefano, G., Poulain, P.-M., Vélez-Belchí, P., Suga, T., Ando, K., Iwasaska, N., Kobayashi, T., Masuda, S., Oka, E., Sato, K., Nakamura, T., Sato, K., Takatsuki, Y., Yoshida, T., Cowley, R., Lovell, J. L., Oke, P. R., van Wijk, E. M., Carse, F., Donnelly, M., Gould, W. J., Gowers, K., King, B. A., Loch, S. G., Mowat, M., Turton, J., Rama Rao, E. P., Ravichandran, M., Freeland, H. J., Gaboury, I., Gilbert, D., Greenan, B. J. W., Ouellet, M., Ross, T., Tran, A., Dong, M., Liu, Z., Xu, J., Kang, K., Jo, H., et al.: Argo Data 1999–2019: Two Million Temperature-Salinity Profiles and Subsurface Velocity Observations From a Global Array of Profiling Floats, Front. Mar. Sci., 7, 2020.

1.7. Terminology

Abbreviation/acronym	Description
AMOC	Atlantic Meridional Overturning Circulation
ATBD	Algorithm theoretical basis document
Argo	International program that uses profiling floats deployed worldwide to observe ocean properties such as temperature and salinity.
BAR	Barystatic sea level
C3S	Copernicus Climate Change Service
COST-G	International Combination Service for Time-variable Gravity Fields
EDD	Experimental Dataset Description
EEH	Expansion efficiency of heat
ESA	European Space Agency
EWH	Equivalent water height
FTP	File transfer protocol
GFZ	Deutsches GeoForschungsZentrum or German research center for geosciences
GIA	Glacial isostatic adjustment
GOHC	Global ocean heat content
GOHU	Global ocean heat uptake
GMHSSL	Global mean halosteric sea level
GMSL	Global mean sea level
GMSSL	Global mean steric sea level
GMTSSL	Global mean thermosteric sea level
GMWTC	Global mean wet tropospheric correction
GRACE(-FO)	Gravity recovery and climate experiment (-Follow on)
GRD	Changes in Earth Gravity, Earth Rotation and viscoelastic solid-Earth Deformation
GSFC	Goddard Space Flight Center
HSSL	Halosteric sea level
IEEH	Integrated expansion efficiency of heat
JPL	Nasa's jet propulsion laboratory
LEGOS	Laboratoire d'Etudes en Géophysique et Océanographie Spatiale
MAN	Manometric sea level
MSS	Mean sea surface

MWR	Microwave radiometer
OHC	Ocean heat content
OHU	Ocean heat uptake
OLS	Ordinary least square
RD	Reference document
SL	Sea level
SLA	Sea level anomaly
SSL	Steric sea level
TSSL	Thermosteric sea level
TUG	Technische Universität Graz or Technical university of Graz

Table 3: List of abbreviations and acronyms

2. Physical principle

In the framework of the MOHeaCAN project, the OHC-EEI product is calculated from regional **OHC change.**

In this document, the word "change" refers to the difference between any two states - it refers to the difference between the present state (t) and the state to a given date (t_{ref}) or time period.

This regional OHC change is derived from the **Steric Sea Level (SSL) change**. For this purpose, a coefficient of expansion efficiency of heat is needed to do the conversion of thermal expansion into OHC change.

2.1. The (Integrated) Expansion Efficiency of Heat

The expansion efficiency of heat (EEH) expresses the change in ocean density due to heat uptake. As a matter of fact it represents the ratio of the temporal derivative of thermosteric sea level over the temporal derivative of the heat content under a given heat uptake. The EEH is dependent on temperature, salinity and pressure (Russell et al., 2000). Thus, integrated over the total water column, the EEH is supposed to vary with latitude along with the variations of integrated salinity, temperature and pressure. At a regional scale, the EEH has never been calculated. To explain this, it occurs that the OHC change over an entire water column can be null whilst the thermal expansion is not. In such a situation, the EEH is not defined and cannot be calculated. A way to avoid this issue is to consider the **integrated expansion efficiency of heat (IEEH)** instead of the EEH (Marti et al., 2022b). In the MOHeaCAN project, the IEEH approach is chosen and allows the conversion of thermal expansion into OHC change. This IEEH coefficient can be retrieved from in-situ measurements. More explanations on the methodology to compute the IEEH coefficient are given in section 3.4..

2.2. OHC change calculation

Theoretically, the thermal expansion is derived from the ThermoSteric Sea Level (TSSL) change. The diagram below presents the relationship between the main variables that are used to calculate the Ocean Heat Content (OHC) change and its time derivative from the TSSL change (obtained from removing the HaloSteric Sea Level (HSSL) change and the Manometric sea level (MAN) change to the total Sea-Level (SL) change) and applying the Integrated Expansion Efficiency of Heat (IEEH) coefficient.

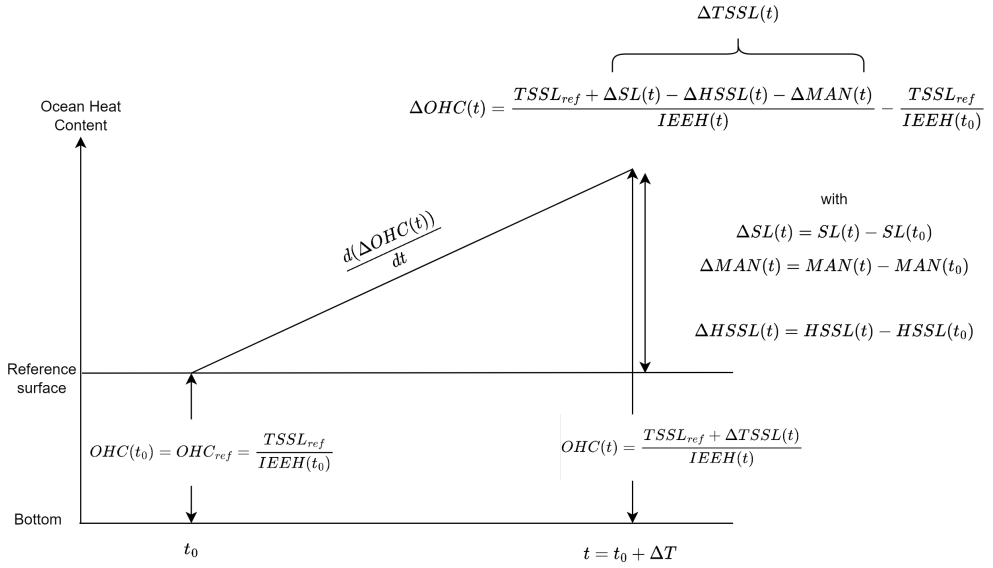

Figure 2: Diagram of OHC change and its time derivative calculation with IEEH approach

OHC change ($\Delta OHC(t)$) is defined by the difference between OHC at t and t_0 , and can be written as follows:

$$\Delta OHC(t) = \frac{TSSL_{ref} + \Delta TSSL(t)}{IEEH(t)} - \frac{TSSL_{ref}}{IEEH(t_0)} \quad \text{Eq. 1}$$

Where $\Delta TSSL$ is the TSSL change, $IEEH$ the integrated expansion efficiency of heat and $TSSL_{ref}$ is the reference of the $TSSL$ at $t = t_0$.

2.3. Comments

2.3.1. Temporal reference of the TSSL

As TSSL change is calculated from SL, MAN and HSSL change (Eq. 2), it is important to note that all these variables have their own reference. If we consider that they have the same reference (i.e. they are all null at $t = t_0$) the following equation applies:

$$\Delta_{t0}TSSL(t) = \Delta_{t0}SL(t) - \Delta_{t0}MAN(t) - \Delta_{t0}HSSL(t) \quad \text{Eq. 2}$$

However, in practice, SL, MAN and HSSL change (see section 3.) are not referenced at the same time or period. If we consider that SL, MAN, and HSSL changes are respectively referenced at $t = t1$, $t = t2$ and $t = t3$ and that the goal is to reference the TSSL change at $t = t0$, we have to apply the following equation for the TSSL change calculation:

$$\Delta_{t0}TSSL(t) = \Delta_{t1}SL(t) - \Delta_{t2}MAN(t) - \Delta_{t3}HSSL(t) - (\Delta SL_{t1}(t0) - \Delta_{t2}MAN(t0) - \Delta_{t3}HSSL(t0)) \quad \text{Eq. 3}$$

With this calculation, we get by construction the TSSL change and the OHC change at t0 equal to 0 whatever the time reference of SL, MAN and HSSL change.

2.3.2. Time derivative of the OHC change

The time derivative of the OHC change is written as:

$$\frac{d(\Delta OHC(t))}{dt} = \frac{d}{dt}\left(\frac{TSSL_{ref}}{IEEH(t)}\right) + \frac{d}{dt}\left(\frac{\Delta TSSL(t)}{IEEH(t)}\right) \quad \text{Eq. 4}$$

It is important to note that the value $TSSL_{ref}$ is important for the calculation of the time derivative of the OHC change and so it is for the calculation of the EEI. The choice of this reference will be further given in the section 4.4.5.3..

2.4. OHC change calculation at the global scale

As this project particularly focuses on the OHC-EEI product defined at the global scale, some approximations can be done.

2.4.1. Estimation from the SSL change

At global scale, the ocean salinity change is negligible (Gregory and Lowe, 2000; Llovel et al., 2019; Gregory et al., 2019). For this purpose, the regional OHC change grids do not need to be derived from the TSSL change but directly from the SSL change grids. The Eq. 1 further becomes:

$$\Delta OHC(t) = \frac{TSSL_{ref} + \Delta SSL(t)}{IEEH(t)} - \frac{TSSL_{ref}}{IEEH(t_0)} \quad \text{Eq. 5}$$

It is important to note that with this method of calculation, variations of OHC change can be locally misrepresented due to the presence of salinity variations in the SSL change. By taking the global mean of Eq. 5, the variations of the salinity can be neglected and the calculation of the global OHC change is done correctly.

2.4.2. Constancy of the IEEH

The IEEH shows regional variations due to ocean temperature and volume changes which may be induced by factors such as ocean currents and atmospheric circulation patterns. However, at the global scale the IEEH can be considered as constant (Eq. 6), with typical trends being less than 0.03% per decade. This means that at the global scale, the ocean is considered a large and well mixed body of water.

$$IEEH(t) = IEEH(t_0) \quad \text{Eq. 6}$$

3. Input data

3.1. Overview

The following section describes the different datasets used for the computation of the OHC change grids. They include time-varying data such as the total SL change, the MAN change and the integrated expansion efficiency of heat, which is used to convert thermal expansion change into ocean heat content change. There is also static data such as the water ratio, grid cells area and the glacial isostatic adjustment. These inputs are spatial data given on the entire globe. However, their spatial availability is different and may vary over time. The origin and format of each dataset are described in a dedicated subsection. The limitations and errors associated with the dynamic input datasets are also presented.

3.2. Manometric sea level

Manometric sea level (MAN) change estimates are derived from gravimetric measurements from 04/2002 to 07/2022. They are extended in the past, going back to 01/1993 with the use of the barystatic sea level (BAR) estimated from the ocean mass budget of the SLBC_cci (Horwath et al., 2022).

3.2.1. Description of gravimetry data

GRACE and GRACE Follow On (GRACE-FO) missions provide the Earth's surface mass changes. As GRACE data are impacted by different error sources (Blazquez et al., 2018; Meyssignac et al., 2019), we used an ensemble approach in order to average the errors and also to evaluate the uncertainty in manometric sea level.

Blazquez et al. (2018) provided an ensemble of MAN solutions derived from GRACE. Spherical harmonics solutions from various processing centers have been considered as those from the Center for Space Research (CSR), the Jet Propulsion laboratory (JPL), the Deutsches GeoForschungsZentrum (GFZ), the Technische Universität Graz (TUGRAZ), the Groupe de Recherche en Géodésie Spatiale (GRGS), and the International Combination Service for Time-variable Gravity Fields (COST-G). These solutions cannot be directly used to estimate the manometric sea level; they need first to be post-processed (Wahr et al., 2004). The post-processing parameters includes (i) the addition of independent estimates of the degree 1 and degree 2 order 0 spherical harmonics (as these harmonics are not observable by GRACE), (ii) a filtering for correlated errors that maps into characteristic north-south stripes, (iii) a correction for the large land signals (from hydrology or glaciers) that can 'leak' into the ocean because of the limited spatial resolution of GRACE, and (iv) a correction for glacial isostatic adjustment (GIA). Blazquez et al. (2018) applied a range of state-of-the-art post-processing parameters to get a spread of GRACE estimates of the manometric sea level. A time mean over 2005–2015 is removed from all GRACE solutions to compute anomalies.

For this study we used an update of the ensemble from Blazquez et al. (2018). The version v1.6 that is used includes new improvements. In comparison with the v1.5 version, we note:

- An increase in the temporal coverage from September 2021 to August 2022
- A reduction of the data gap between GRACE and GRACE-FO.
- Two corrections were added: one for the earthquakes (Tang et al., 2020) and one for the ocean mass change for the first 300km near Greenland and Antarctica.
- The processing centers which are used are CSR, GFZ, JPL RL06, TUGRAZ 2018 and CNES5.0
- Only two geocenters solutions are used (Processing of SLR Observations at CNES., 2020; Sun et al., 2016)
- A correction of an issue associated with the Love numbers has been applied and the associated GIA correction have been updated
- The coefficient associated to degree 2 and order 0 from the Processing of SLR Observations at CNES (2020) is not only anymore estimated from SLR data but from the combination of SLR and GRACE data

3.2.2. Description of the barystatic sea level from SLBC_cci

The barystatic component of the sea level from SLBC_cci (Horwath et al., 2022, RD7) is estimated by summing several contributions:

- The contribution from global glacier mass changes assessed by a global glacier model
- The contribution from Greenland Ice Sheet mass changes assessed by satellite radar altimetry and by GRACE
- The contribution from Antarctic Ice Sheet mass changes assessed by satellite radar altimetry and by GRACE
- The contribution from terrestrial water storage anomalies assessed by the global hydrological model WaterGAP (Water Global Assessment and Prognosis)

3.2.3. Concatenation of the data

To concatenate the SLBC_cci and GRACE data we propose to put the SLBC_cci global data in the same format as the GRACE regional grids. To do so we project the values of the SLBC_cci global data on regional grids. This procedure has to be followed for each one of the 120 solution in the GRACE ensemble:

- The first step consists in estimating the global mean of the GRACE data solution
- Thus the annual signal of the GRACE solution is calculated over the period 2002-2012 and removed
- A regression is computed separately on SLBC_cci and GRACE data (2002-2012)
- An offset is estimated between both regressions in 04/2002
- The offset is removed from SLBC_cci data over the period 1993-2002
- SLBC_cci data (1993-2002) is concatenated together with GRACE data (2002-2022) and the annual signal of GRACE is added back on the full period
- The SLBC_cci data is projected on the GRACE grid with the same value at each grid point per month

By following this procedure, it allows to generate a set of 120 manometric solutions over the period 1993-2022. The results of the concatenation in terms of barystatic sea level is shown in the Figure 3

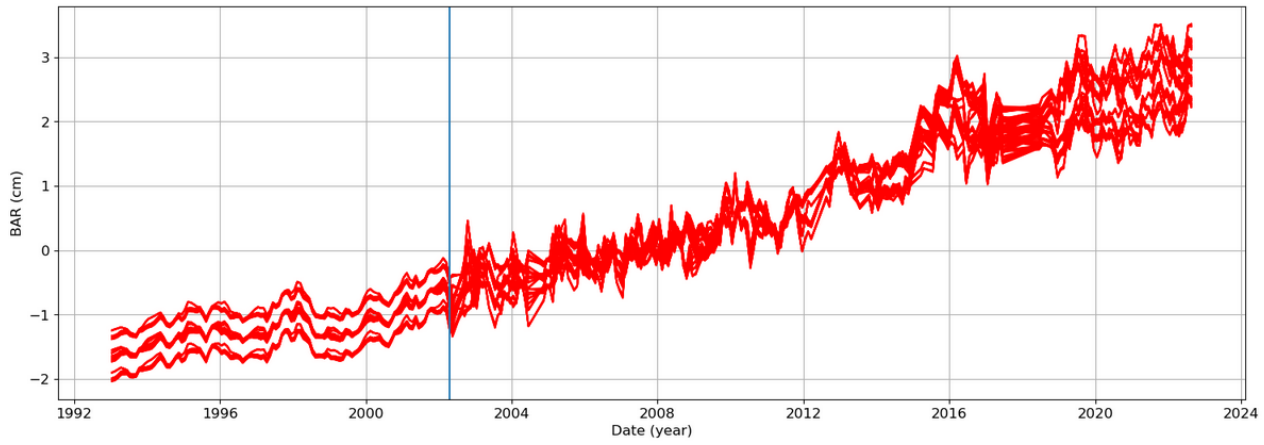

Figure 3 : Timeseries of all the solutions of the barystatic sea level after the concatenation. The removal of the annual signal was done prior to plotting. The vertical blue line represents the date at which the concatenation between GRACE and SLBC_cci data is done.

The MAN data content is described below:

- Ensemble of 120 MAN solutions and its ensemble mean
  - units: m equivalent water height (EWH)
  - spatial resolution: global (prior 04/2002) and 1° x 1° afterwards
  - temporal resolution: monthly
  - temporal availability: January 1993 - August 2022
  - version: v2.2 (SLBC_cci) & v1.6 (GRACE)

3.2.3. Comments/limitations

First, it is important to note that at global scale, we use the definition of Barystatic sea level rise (BAR) instead of global mean of manometric sea level change (Gregory et al., 2019)

As explained in Blazquez et al. (2018), the combination of the different raw solutions (from processing centers) with the different post-processing parameters (geocenter motion correction, filtering techniques, leakage and GIA corrections) leads to an ensemble which is assumed to cover a significant part of the uncertainty range of GRACE/GRACE-FO manometric sea level estimates.

For this reason, the entire 120 solutions ensemble is used to estimate the MAN uncertainties at global scale (see section 5.4.2.).

Concerning the SLBC_cci data, as it is given at the global scale, it is then considered homogeneous over the global ocean. The hypothesis behind this approximation is motivated by the fact that the contribution of the mass term to spatial variations of SL change is only significant in closed seas and high latitudes (Piecuch and Ponte, 2011; Piecuch et al., 2013).

3.3. Sea level

3.3.1. Description

Sea level change at regional scales are derived from the sea-level products operationally generated by the Copernicus Climate Change Service (C3S). This dataset, fully described in (Legeais et al., 2021) is dedicated to the sea level stability for climate applications. It provides daily sea-level anomalies grids based at any time on a reference altimeter mission (TopEx/Poseidon, Jason-1,2,3 and S6-MF very soon) plus a complementary mission (ERS-1,2, Envisat, Cryosat, SARAL/Altika) to increase spatial coverage.

C3S provides the sea level anomaly (SLA) around a mean sea surface (MSS) above the reference mean sea-surface computed over 1993-2012, or in other words, the total SL change [Table 2, RD2]. Data is available in NetCDF format files on the C3S data store [Table 2, RD1]. The main characteristics of SLA grids are:

- spatial resolution: 0.25° x 0.25°

- temporal resolution: daily
- temporal availability: altimetry era, January 1993 - May 2022
- units: m
- version: vDT2021

More information is available in the product user manual of C3S [RD2].

3.3.2. Comments/limitations

C3S data result from the most up-to-date standards (altimeter standards, geophysical corrections) whose timeliness is compatible with the C3S production planning and most of them follow the recommendations of the ESA Sea Level CCI project. They are submitted to a rigorous validation process.

However, these data are affected by errors like any spatial measurements. The full description of these errors was described by Ablain et al., (2015, 2019) and (Guérou et al., 2022). In this study, a variance-covariance matrix dedicated to the description of the global mean sea level (GMSL) error was provided (Ablain et al., 2018). This error matrix is also well adapted to the description of C3S data measurements because the GMSL errors are the same (similar altimeter standards). It has therefore been used as an input for the error propagation purpose in this project (see section 5. devoted to this topic).

3.3.3. Specific corrections

Grids of sea level change provided by C3S do not take in consideration the global isostatic adjustment (GIA) process in response to the melting of the Late Pleistocene ice sheets. However, this effect needs to be corrected in sea level change estimates as it does not reflect the ocean's response to recent climate change. GIA contains regional variations that must be corrected. It is still an area of active research, and then several GIA grids expressed as trends in lithospheric height change (in mm/year) are available in the literature. The same GIA correction used in the recent study (Prandi et al., 2021) for an estimation of the sea level trends uncertainties at regional scale has been applied. It is an ensemble mean of the regional GIA results for model ICE-5G, with various viscosity profiles (27 profiles) (see Figure 4). The methodology is also described in Spada and Melini (2019). The average GIA value over oceans from this 27 solution ensemble is 0,33 $mm.yr^{-1}$ closely matching the value of -0.3 $mm.yr^{-1}$ (WCRP Global Sea Level Budget Group, 2018), generally adopted as a rule of thumb to correct the altimetric absolute sea-level trend for the effects of past GIA.

An additional correction is considered to take into account the ocean bottom deformation due to present-day mass redistribution. This correction GRD (changes in Earth Gravity, Earth Rotation and viscoelastic solid-Earth Deformation) has been evaluated at 0.1 mm/yr during the altimetry area (1993-2014), (Frederikse et al., 2017). We have applied this correction only on sea level observations because this effect has no impact on the gravimetric data. The constant value is used in the regional computation.

Moreover, recent studies have shown that a drift on Jason-3 radiometer data has been detected and a correction should be applied on sea level grids. This correction was calculated from the relative differences between the global mean wet tropospheric correction (GMWTC) from Jason-3 microwave radiometer (MWR) and the GMWTC derived from water vapour climate data records (Barnoud et al., 2023a), the GMWTC from SARAL/AltiKa's MWR and the GMWTC from Sentinel-3A. The correction C_{J3} is computed as the average of the zero-mean GMWTC differences (Barnoud et al., 2023b), it is therefore homogeneous over the global ocean.

Between 1993 and 1998, the global mean sea level has been known to be affected by an instrumental drift in the TOPEX-A measurements which has been quantified by several studies (Watson et al., 2015; Dieng et al., 2017). A correction for the instrumental drift has been applied on the sea level grids (Ablain et al., 2017). The correction C_{TPA} is estimated at the global scale and considered homogeneous over the global ocean.

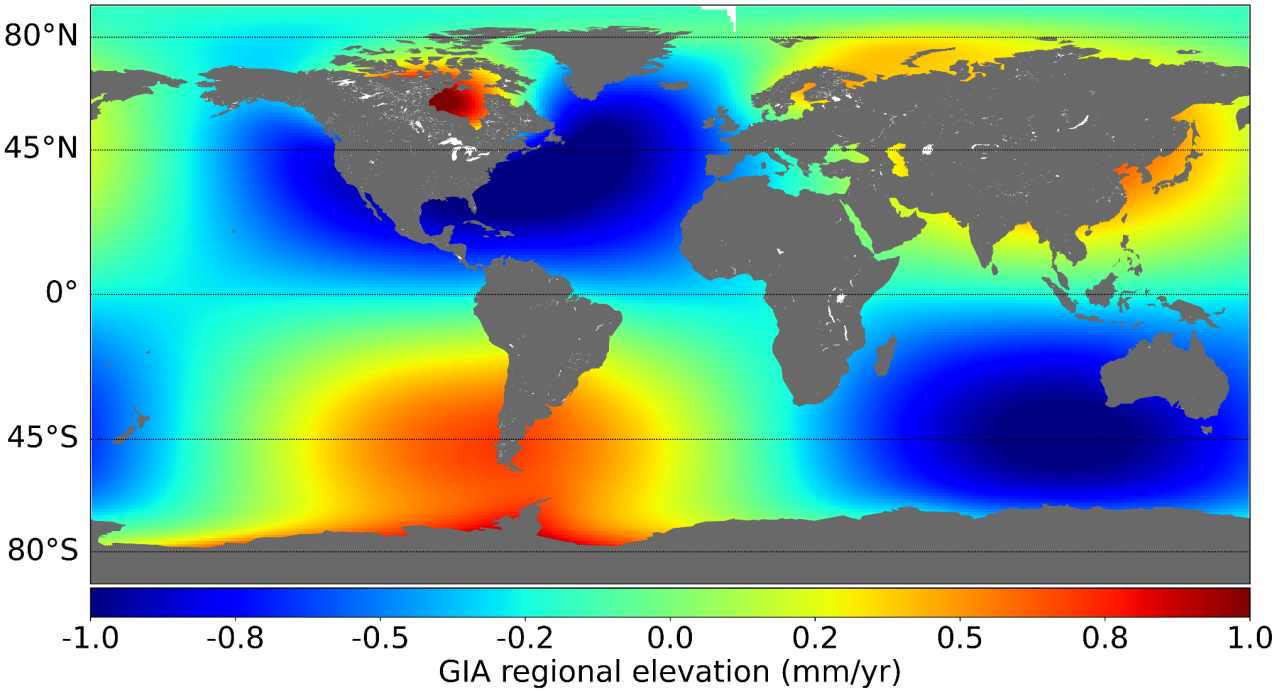

Figure 4 Regional grid of the GIA correction applied to altimetry sea level grids in MOHeaCAN processing chain (Spada and Melini, 2019)

3.4. Integrated Expansion Efficiency of Heat

3.4.1. Description

The integrated expansion efficiency of heat (IEEH) expresses the ratio between the thermosteric sea level change and the ocean heat content change.

3.4.2. Regional estimates of the integrated EEH

In the framework of this project, IEEH values are provided as 3D grids defined at regional scales with a 1-degree spatial resolution and at monthly timescale. They are calculated based on in situ temperature and salinity fields. IEEH is defined as the ratio between TSSL change and OHC change:

$$IEEH(t, lat, lon) = \frac{\Delta TSSL(t,lat,lon)}{\Delta OHC(t,lat,lon)} \quad \text{Eq. 7}$$

where :

- ΔTSSL(t,lat,lon) is the thermosteric sea-level change of the whole water column referenced to a physical thermosteric sea-level content (defined at 0° Celsius and 35 PSU) and calculated from in-situ measurements of temperature and salinity following:

$$\Delta TSSL(t, lat, lon) = [\Sigma_j \frac{(\rho_{ref} - \rho(T, S_{clim}, \Sigma_i h_i)).|h_j|}{\rho_{ref}}](t, lat, lon) \quad \text{Eq. 8}$$

- ΔOHC(t,lat,lon) is the ocean heat content change integrated over the whole water column and is calculated following:

$$\Delta OHC(t, lat, lon) = [\Sigma_j \ \rho(T, S, \Sigma_i h_i).C_p(T, S, \Sigma_i h_i).CT(T, S, \Sigma_i h_i).\ |h_j|](t, lat, lon) \quad \text{Eq. 9}$$

Where

- h_j is the j-th value of the thickness layer so that $\Sigma_i h_i$ is the depth of integration (in m),
- ρ_{ref} is the reference value of the density computed at fixed Salinity (35psu) and Temperature (0°C),
- $\rho(T, S, \Sigma_i h_i)$ is the density calculated based on salinity and temperature variations,
- $\rho(T, S_{clim}, \Sigma_i h_i)$ is the density with salinity fixed at the climatology,
- $CT(T, S, \Sigma_i h_i)$ is the conservative temperature (in $°C$) and,
- $C_p(T, S, \Sigma_i h_i)$ is the heat capacity of sea water (in $J.kg^{-1}.°C^{-1}$)

Note that $TSSL$ and OHC changes are locally filtered with a cutoff period of 3 years before estimating the IEEH. This high-frequency variability can arise from various sources, such as local weather conditions, ocean currents, and internal ocean waves. These high-frequency signals can mask the underlying signal of interest, which is the long-term trend in ocean thermal expansion that reflects the IEEH. In this way, the IEEH coefficient gives the OHC for the whole water column for a variation of thermosteric sea level around a physical reference. ECCO dataset [RD6] is used to compute the $TSSL$ change and OHC change over 0-6000 m depth. Afterwards we can take the time-mean of the time varying IEEH over a chosen period to estimate the time-mean IEEH which is used to estimate the OHC change.

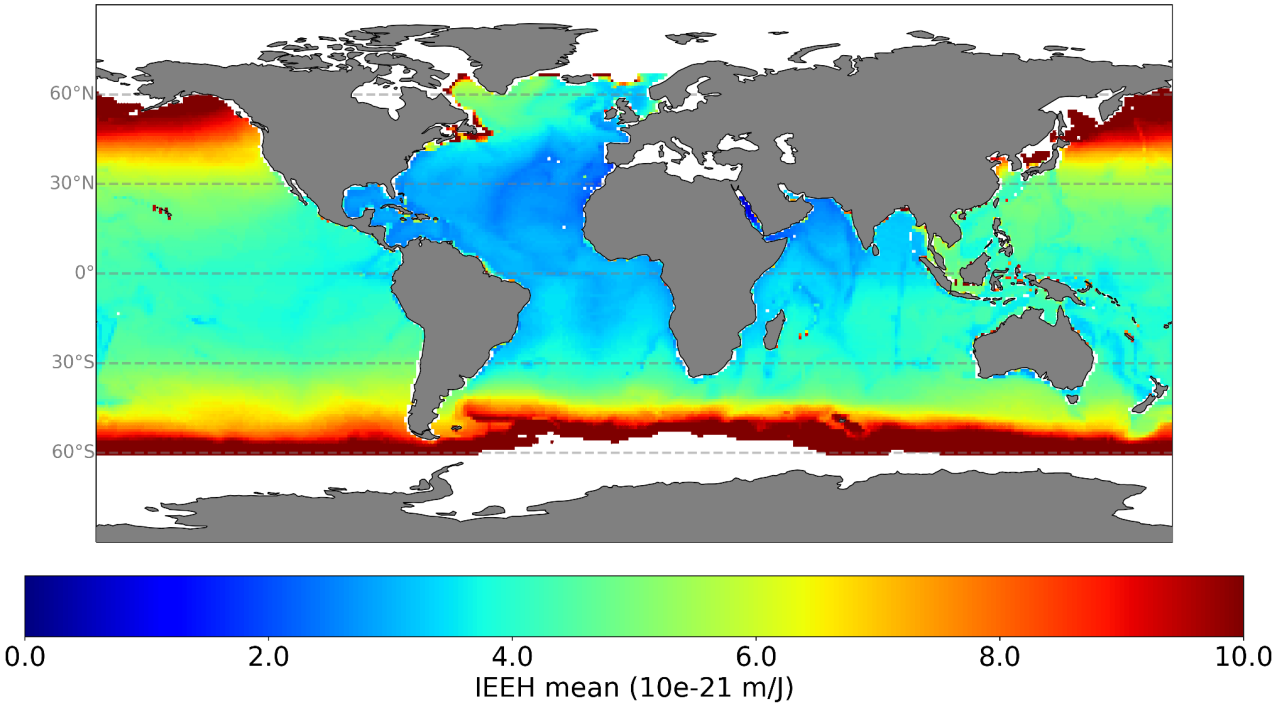

Figure 5 Time-mean of the Integrated Expansion Efficiency of Heat (IEEH) coefficients (10^{-21} m/J) (1x1 degree).

Finally, the main characteristics of IEEH grids are:

- spatial resolution: 1° x 1°
- temporal resolution: monthly
- depth integration: ECCO-V4r4 data [RD6] for the 0-6000m depth (Forget et al., 2015; ECCO Consortium et al., 2020).
- temporal average: January 2005 - December 2015
- units: m/J

3.4.3. Comments/limitations

To assess the uncertainties on the OHC and EEI derived from data at global level, both the value and the uncertainty on the global IEEH are required. The one which is used in this project is provided by Marti et al. (2022). It is significantly lower than errors obtained by Kuhlbrodt and Gregory (2012) and Church et al. (2011).

3.5. Static data: water ratio

When manipulating data at regional scales, it is necessary to know the proportion of ocean in each cell for grid's downsampling or deriving the global mean for instance.

A water ratio grid is computed from distance to coast information and provides the part of water surface in each cell of the grid between 0 and 1. Distance to coast data is provided by the NASA Goddard Space Flight Center (GSFC) Ocean Color Group and given on a 0.01° resolution grid.

3.6. Static data: grid cells area

When manipulating data at regional scales, it is necessary to know the area of each cell for grid's downsampling or deriving the global mean for instance. The surface is computed for each grid cell taking the Earth oblateness into consideration.

4. OHC and EEI processing chain

4.1. Outline

In the MOHEACAN processing chain, the EEI is deduced from the Global Ocean Heat Uptake (GOHU) which is a very good approximation since the oceans store 91% of the heat kept by the Earth system (IPCC, Forster et al., 2021).

The GOHC is itself estimated from space data from altimetry and gravimetry missions (GRACE and GRACE-FO). In the MOHeaCAN project, the GOHC is obtained from regional grids.

As the OHC is computed from altimetry and gravimetry spatial observations, its spatial and temporal characteristics depend on these measurements. However the derived OHC characteristics are only limited by gravimetry observations both at spatial and temporal scales. Indeed, the effective temporal and spatial resolutions of GRACE(-FO) products is 1 month and 300 km against about 10-days at about 100 km for level-4 altimetry products. Therefore the regional OHC grids in the MOHeaCAN project have been defined at 1°x1° resolution and on a monthly basis. The EEI is derived from the temporal derivative of the GOHC after filtering-out the high-frequency signals lower than 3 years in order to assess the long-term EEI variable.

For reminder, the variables noted SL and MAN in this document are not absolute quantities but anomalies with respect to a reference (see sections 3.2. and 3.3.). SSL and OHC variables and the global variables (GMSL, BAR, GMSSL, GOHC) are therefore also anomalies.

The Figure 6 below describes the MOHeaCAN processing chain with its main algorithms for generating OHC/EEI data from input altimetry and gravimetry data. The following subsections describe the algorithms developed in detail.

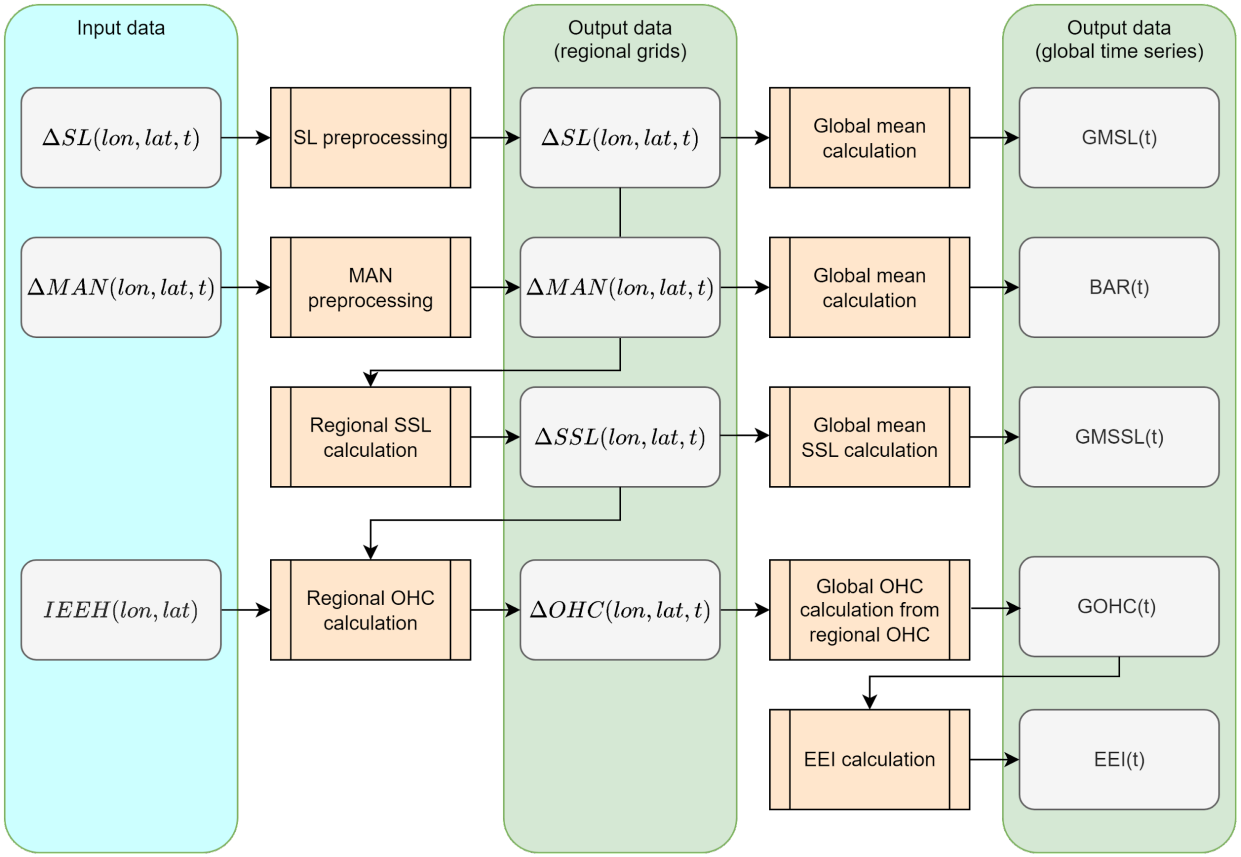

Figure 6 Overview of the MOHeaCAN processing chain. Variables are given with their dimensions (lon: longitude, lat: latitude, t: time). Global mean time series (GMSL, BAR, GMSSL) are computed but do not intervene in the GOHC/EEI calculation afterwards.

4.2. Basic underlying assumptions

The OHC is a good proxy for EEI

As the majority of the excess of energy held back in the Earth system is stored by the oceans (91%), the ocean heat content is assumed to be a reliable gauge to monitor the energy budget of the system. In this project, we assume the land, atmosphere and cryosphere reservoirs contribute 9% to the energy storage at large time scales.

The space geodetic methodology allows the estimation of the steric sea level changes due to thermal expansion (thermosteric) and salinity variations (halosteric)

Variability in ocean salinity yields sea level changes mainly at regional scales, at global scale the ocean salinity variations can be neglected.

The EEI is defined as the flux of excess/deficit of energy measured on top of the atmosphere

GOHC and EEI variables are defined in relation to a reference surface, localised 20 km above the sea level. This reference level has been assumed for defining satellite-based TOA fluxes (Loeb et al., 2018).

4.3. Input data

The MOHeaCAN processing chain, which allows to compute the OHC change and EEI variables, is configured to use the following input data, described in section 3.

- MAN change gridded data (spatial resolution: 1°x 1° - temporal resolution: monthly)
- SL change gridded data (spatial resolution: 0.25°x 0.25° - temporal resolution: daily)
- Time-mean IEEH gridded data (spatial resolution: 1°x 1° - temporal resolution: monthly)
- land mask (spatial resolution: 1° x 1°)

4.4. Output data

The MOHeaCAN main product contains the OHC-EEI produced by the processing chain and described in Figure 6 for each month from April 2002 to December 2020:

- Global OHC time data series
- EEI (after applying a low-pass 3 year filtered period on OHC and GOHC)
- Error variance-covariance matrices of GOHC and EEI
-
- GOHC and EEI quality flags (which indicates the data that are interpolated, due to the lack on gravimetric data between GRACE and GRACE-FO)

The format of the MOHeaCAN product is described in detail in the product user manual (PUM [AD1]).

An additional product is available upon request which contain other variables, mainly the intermediate variables (cf PUM [AD1]).

4.5. Retrieval methodology

4.5.1. Overview

The algorithms applied in the MOHeaCAN processing chain are described in the following subsections in agreement with Figure 6:

- the preprocessing of regional SL change grids
- the preprocessing of regional MAN change grids
- the calculation of regional SSL change grids
- the calculation of regional OHC grids

- the calculation of the global mean of SL, MAN and SSL change grids to get the GMSL, BAR, GMSSL time series
- the calculation of the GOHC from the OHC change grids
- the calculation of the EEI.

For each algorithm, the objectives, the main mathematical statements and the limitations and any comments about the approach are presented.

4.5.2. Preprocessing of SL change grids

4.5.2.1. Description

The objective of the preprocessing of the SL change grids is to modify the temporal and spatial resolutions of SL change grids used as input data. Indeed, altimetry data used in the MOHeaCAN processing chain is provided by C3S and are given on a daily basis at 0.25x0.25 degrees resolution. Altimetry data need to be downsampled to 1x1 degrees resolution and at the monthly time step to be compared to MAN change and HSSL change grids.

Moreover, the sea level regional grids from C3S are not corrected from the glacial isostatic adjustment (GIA), the elastic effect of the contemporary land ice melting (GRD), Jason-3 drift and TPA drift. To estimate OHC change, these specific corrections must be applied.

4.5.2.2. Mathematical statement

4.5.2.2.1. Temporal interpolation

In order to calculate the SL change grids on a monthly basis (i.e. to switch from a daily to a monthly temporal resolution), a basic average of the N grids of the month is performed. Cells with default values are not taken into account. The monthly averages are kept for each cell regardless of the number of valid values over the month.

4.5.2.2.2. Spatial filtering

The monthly grids are first spatially filtered with a lanczos filter along the longitude and latitude coordinates. The cut-off length is chosen at 150km and allows to filter out high frequency spatial scales in the sea level which are not present in the gravimetry and halosteric datasets.

4.5.2.2.3. Spatial interpolation

The monthly grids are then computed at a higher spatial resolution: 1x1 degrees instead of 0.25x0.25 degrees. The method applied consists in applying an average of the 4 cells located at the center of a box composed of 16 cells after the application of the Lanczos filter on the grids. This average will be the new value of the full 16 cells box which is 1° sided.

4.5.2.2.4. Corrections applied

Several corrections are applied to the sea level change grids (see section 3.3.3.). The GIA unstructured ensemble mean grid is first sampled on a regular 1 degree resolution grid using linear interpolation. Regional sea level change grids are finally corrected from the GIA correction, the GRD correction, the Jason-3 drift and the TPA drift:

$$\Delta SL(x,y,t) \; - \; GIA(x,y) \; - \; GRD(x,y) \; - C_{J3}(t) - C_{TPA}(t) \qquad \text{Eq. 10}$$

4.5.2.3. Comments/limitations

With regards to the GIA correction, it is still an area of active research. However the impact at regional scales is mainly significant at high latitudes (e.g. discrepancies can reach 0.5-1 mm/yr) where, for the moment, limited information is provided in the MOHeaCAN product due the application of a restrictive geographical mask based on the IEEH estimated with ECCO model (see below for more details).

With regards to the Jason-3 drift and TPA corrections, they were derived to correct the global mean SL. Here an approximation is made by applying these corrections at regional scales.

4.5.3. Preprocessing of MAN change grids

4.5.3.1. Description

Gravimetry data used in the MOHeaCAN processing chain are provided at 1°x 1° resolution and monthly time step. MAN change grids are already at a good spatial and temporal resolution. Hence, the objective of the preprocessing of the MAN change grids is to fill the data gaps of the GRACE(-FO) in the manometric sea level change grids.

4.5.3.2. Mathematical statement

4.5.3.2.1. Management of the data gap

The MAN change grids contain several gaps due to degradation of the operational capability of GRACE and GRACE-FO and the transition time between the two missions. An implementation of a gap filling algorithm has been made in the product chain generation. This algorithm is described as follows:

- Calculation of the climatological signal: removal of the trend and calculation of the average for each month of the year
- Removal of the climatological signal over the whole time series
- Cubic approximation of the time series to fill in the gaps
- Adding the climate signal to the whole time series (including the gap)

This gap filling algorithm has been applied at regional scales, i.e for each element of the MAN change grids.

An important feature brought by the gap algorithm to the OHC change product is a quality flag which distinguishes between months for which there is data from observations and those for which there is data from interpolation of MAN change. A more detailed explanation of this quality flag is given in the PUM [AD1].

4.5.3.2.2. Addition of a high frequency component into the data gaps

The gap-filling algorithm underestimates the part of the signal driven by sub-annual processes. By construction, the high frequency content of the BAR uncertainty estimates in the data gaps are also underestimated. To deal with that problem, prior to the calculation of the variance-covariance matrix (section 5.4.2.), some modifications were directly made onto the

signals of the ensemble of manometric sea level solutions. The high frequency related signal component was added to the ensemble signals as follows:

- Application of a 1-year filter onto MAN data with prior removal of the annual and semi-annual components of the signal
- Calculation of the standard deviation of the difference between the initial and filtered MAN signal
- Stochastic addition with a normal (Gaussian) distribution of this residual standard deviation at the locations where the MAN is suffering from a lack of data

Note that this method is applied to all the data gaps on the full time period.

4.5.3.3. Selection of a subset of the ensemble

The concatenation of GRACE data with SLBC_cci data simply results in the compensation of an offset on the barystatic sea level in 04/2022 (section 3.2.3.). In addition to this, it has been chosen to use a subset of solutions in the GRACE ensemble that most closely resemble the SLBC_cci data in terms of trend of the barystatic sea level over the period 2002-2016. This is because to date the SLBC_cci component of mass is the reference dataset for the closure of the sea level budget (Horwath et al., 2022). The subset of BAR solutions used to estimate the OHC-EEI product are the average of half of the solutions of the GRACE ensemble which turn out to be the solutions that were calculated with the geocentre of Sun et al. (2016).

4.5.3.4. Comments/limitations

The spatial interpolation method applied is simple. More sophisticated algorithms could be applied to account for data gaps in the time series. Such methods based on the filter approach (e.g. Gaussian filter for spatial interpolation) are planned in future versions of the OHC change products. The impact on these improved algorithms is unknown at this time.

4.5.4. Calculation of regional SSL change grids

4.5.4.1. Description

The objective is to calculate the regional SSL change grids from SL and MAN change grids. The relationship between sea level change (ΔSL), manometric sea level change (ΔMAN) and steric sea level change (ΔSSL) is expressed by the sea level budget equation:

$$\Delta SL = \Delta SSL + \Delta MAN \qquad \text{Eq. 11}$$

4.5.4.2. Mathematical statement

The SSL grids are obtained from the difference between SL and MAN grids at each time step. As SL and MAN grids have been preprocessed at same spatial and temporal resolution, the differences between grids is straightforward:

$$\Delta SSL(lon, lat, t) = \Delta SL(lon, lat, t) - \Delta MAN(lon, lat, t) \quad \text{Eq. 12}$$

For each cell containing a default value in the SL and MAN change grids, a default value is assigned in the SSL change grids.

4.5.4.3. Comments/limitations

Other alternative methodologies are used to derive the steric sea level grids. They rely on in situ data instead of spatial data, mainly from temperature and salinity profiles provided by the Argo network. The advantages and inconvenients of such an approach is presented in Meyssignac et al. (2019).

At global scale, when corrected for changes in manometric sea level, sea level change provides an estimate of the thermal expansion of the ocean. This assumption is less true at regional scales as we can not neglect salinity variations anymore (Gregory and Lowe, 2000; Llovel et al., 2019; Gregory et al., 2019). Theoretically at regional scales, halosteric sea level change estimates should be removed from the steric sea level change retrieved from the space geodetic approach. However, recent studies highlight that in situ salinity datasets from Argo present a drift from 2016 due to anomalies on the conductivity sensors (Wong et al., 2020). Barnoud et al. (2021) showed that this affects the HSSL estimates. To avoid the impact of this halosteric drift from in situ measurements on the MOHeaCAN product, it has been decided to neglect the removal of the halosteric component at regional scales.

Steric sea level is obtained by subtraction of signals. Some limitations related to this operation can be identified. The GIA datasets used to correct the gravimetry signals and the sea level from altimetry are not consistent (three different GIA corrections for the post-processing of gravimetry solutions and one solution for altimetry, see sections 3.2. and 3.3.3.). To date, the impact of such incoherency in the processing of data is expected to be low. However, a possible homogenisation of the pre-processing of altimetry and gravimetry datasets should solve this issue. Finally, the dynamical atmospheric correction based on MOG2D model (Carrère and Lyard, 2003) has been removed in altimetry processing whereas only the inverse barometer correction has been applied in gravimetry processing (Blazquez et al., 2018). The impact of this discrepancy must be studied and corrected if needed.

4.5.5. Calculation of regional OHC change grids

4.5.5.1. Description

The objective is to calculate the regional OHC change grids from SSL grids at the same spatial and temporal resolution. Once the IEEH variable is determined at regional scale, SSL change is translated to OHC change thanks to the IEEH at every timestep.

4.5.5.2. Mathematical statement

In order to get the ocean heat content change (in Joules), we divide all grids of steric sea level changes (m) by the regional IEEH grid ($m.J^{-1}$) by considering a time or period of reference t_{ref}

(see section 2.2.). According to the Eq. 5 given in section 2.4, the OHC change is expressed per unit of area (J.m^{-2}) once it is divided by the reference surface:

$$\Delta OHC(lon,lat,t) = \frac{\Delta SSL(lon,lat,t)+TSSL_{ref}(lon,lat)}{surf_{ref}(lon,lat)*IEEH(lon,lat)} - \frac{TSSL_{ref}(lon,lat)}{surf_{ref}(lon,lat)*IEEH(lon,lat)} \quad \text{Eq. 13}$$

where $surf_{ref} = 4\pi * (R + h_{TOA})^2$ is defined as the surface of the Earth at the top of the atmosphere, for a reference height of the top of the atmosphere at 20 km altitude ($h_{TOA} = 20.10^3\, m$), with R the radius of the Earth ($R = 6371.10^3\, m$) (see section 4.2), and where $TSSL_{ref}$ is assumed to be equal to SSL_{ref} (see section 2.4. and section 4.5.4.3.).

It results in monthly OHC change given on a 1°x1° resolution grid. For each cell containing a default value in the SSL or IEEH grids, a default value is assigned in the OHC grids.

4.5.5.3. Comments/limitations

The OHC change calculation requires a reference value for the TSSL/SSL. In order for this reference value to be consistent with the IEEH value in Eq. 13, thus $TSSL(t = 01/2005, lat, lon) = TSSL_{in-situ}(t = 01/2005, lat, lon)$. A sensitivity study has been led on the choice of the date or period of reference and the associated $TSSL_{ref}$ value. The results have shown no significant impact on the OHC change calculation and the time derivative of the OHC change.

The grid containing the regional IEEH coefficients was calculated from the temperature and salinity profiles derived from the ECCO model. Consequently, this grid is now defined near coastal areas (>100 kms) since the model dynamic is effective at those locations where there are few observational constraints from Argo data but still, some more work needs to be done to include higher latitudes.

4.5.6. Calculation of the global mean time series for the GMSL, BAR and GMSSL

This section aims at describing the calculation of the global mean time series of the GMSL, BAR and GMSSL from the regional grids. These global variables are provided in the final OHC-EEI product for information but are not used in the global OHC computation.

4.5.6.1. Description

The objective is to calculate the global mean time series of SL, MAN and SSL from SL, MAN and SSL change grids calculated after being preprocessed in space (1x1 degrees) and time (monthly time step).

4.5.6.2. Mathematical statement

At each time step (monthly), the global average (GMSL, BAR or GMSSL) of each grid (1x1 degrees) is calculated by performing a weighted average taking into account the sea surface of each cell. The weighting grid (w) takes into consideration the surface area of each cell but also

the water/land ratio. Below the mathematical formulation for the GMSL (exactly the same for BAR and GMSSL):

$$GMSL(t) = \frac{1}{N*N'} \frac{\sum_{i=1}^{N}\sum_{j=1}^{N'} w(lon_i,lat_j)*SL(lon_i,lat_j,t)}{\sum_{i=1}^{N}\sum_{j=1}^{N'} w(lon_i,lat_j)} \quad \text{Eq. 14}$$

Moreover, in order to be consistent with the calculation of the regional OHC, a mask where the coefficients of the IEEH grid are defined is first applied before calculating the global average of the grids.

4.5.6.3. Comments/limitations

The GMSL, BAR and GMSSL time series are calculated on the limited area provided by the IEEH coefficient grid. As the IEEH coefficient grid covers about 87% of the ocean surface, the time series calculation does not represent the full ocean coverage. The impact of this limitation is under investigation.

4.5.7. Calculation of the global time series for the GOHC from the OHC grids

4.5.7.1. Description

The objective is to compute the global OHC time series (GOHC) from the OHC grids previously computed at the same time step (monthly). As the OHC is not an integrative variable, the global OHC is not derived from the global average of OHCs as for the GMSL or BAR time series, but is simply deduced by summing the valid OHC values from each OHC grid of each time step.

4.5.7.2. Mathematical statement

The GOHC ($J.m^{-2}$) time series is the sum of each OHC cell for each OHC grid at each time step (monthly) for valid values only (default values are ignored):

$$GOHC(t) = \sum_{i=1}^{N}\sum_{j=1}^{N'} OHC(lon_i, lat_j, t),\ for\ t \in [t_0, t_n] \quad \text{Eq. 15}$$

4.5.7.3. Comments/limitations

The propagation of uncertainties is, for the moment, carried out only from a global approach. Thus the GOHC calculated from the regional approach does not yet contain the associated uncertainties (see section 5. on uncertainties estimation). It is also for this reason that we have maintained a global approach in the processing chain.

4.5.8. Calculation of the EEI

4.5.8.1. Description

The Global Ocean Heat Uptake (GOHU) corresponds to temporal variations of the GOHC, it represents almost 91% of the EEI. It is therefore simply inferred from the time derivative of the GOHC on a monthly basis. However, it appears that prior to the calculation of the GOHC, OHC change grids contain regional high-frequency signals which are not related to the EEI imbalance. Firstly, OHC change grids contain high-frequency signals (< 2-3 years) which are due to errors in spatial gravimetry measurements but also in altimetry measurements (e.g. phase shift of the annual signals between these measurements). Moreover, the OHC change grids also contain a residual signal (< 2-3 years) related to the ocean variability at small temporal scale but not related to ocean warming due to climate change. For these reasons it is necessary to filter out these high-frequency signals lower than 3 years.

4.5.8.2. Mathematical statement

EEI is calculated from these following steps:

- the OHC grids are smoothed using a low pass filter (Lanczos) with a cut-off period at λ=3 years.
- mean annual and semi-annual cycles are removed from the GOHC time series after estimating these both signals by applying a least square method
- the adjusted GOHC signal is smoothed using a low pass filter (Lanczos) with a cut-off period at λ=3 years.
- GOHU is calculated from the temporal derivative of the filtered and adjusted GOHC time data series:

$$GOHU(t) = \frac{dGOHC_{filtered,\,adjusted}(t)}{dt},\ for\ t \in [t_0, t_n] \quad \text{Eq. 16}$$

- Since GOHU represent 91% of the EEI, we can obtain the EEI with:

$$EEI(t) = GOHU(t) * \frac{1}{\alpha},\ with\ \alpha = 0.91 \quad \text{Eq. 17}$$

$$EEI \approx \frac{1}{\alpha} \frac{d\,GOHC}{dt} \quad \text{Eq. 18}$$

4.5.8.3. Comments/limitations

Even if OHC change grids have been filtered prior to the calculation of the GOHC, some high-frequency signals below 3 years could subsist in the sum of the regional OHC due to

aliasing. Thus, it is necessary to filter out the high-frequency content of the GOHC with a cut-off period at λ=3 years to remove these potential high-frequency signals.

The computation of the temporal derivative is made by applying a central finite difference scheme on the signal:

$$GOHU(t) = \frac{GOHC_{filtered,\,adjusted}(t+1) - GOHC_{filtered,\,adjusted}(t-1)}{2*dt},\ for\ t \in [t_1, t_{n-1}] \quad \text{Eq. 19}$$

Except for $t = t_0$ where we use the forward finite difference scheme and for $t = t_n$ where we use the backward finite difference scheme.

5. Uncertainties calculation and propagation

5.1. Overview

In parallel to the product processing described in the previous section, the uncertainties are calculated and provided for all the global time series: GMSL, BAR, GMSSL, GOHC and EEI. The proposed approach consists in providing a variance-covariance matrix (Σ) of the errors for each time series. Once the variance-covariance matrices are known, the trend uncertainties can be derived for any time-spans over each time series. It is also possible to make it for any other indicators such as the mean, the acceleration or the magnitude of the annual signals for instance. The method is based on the study performed by Ablain et al., 2019 dedicated to the GMSL trend and acceleration uncertainties.

At this stage of the MOHeaCAN project, the uncertainties are not provided at regional scales. Such regional uncertainties have been already provided by Prandi et al. (2021) for the sea level trends and accelerations, but work is still necessary to generalise the approach for other variables, and also to account for the spatial correlation of the errors.

The Figure 7 below describes main steps to propagate the uncertainties from the GMSL and BAR times series until the GOHC and the EEI . The following subsections described the algorithms developed in detail.

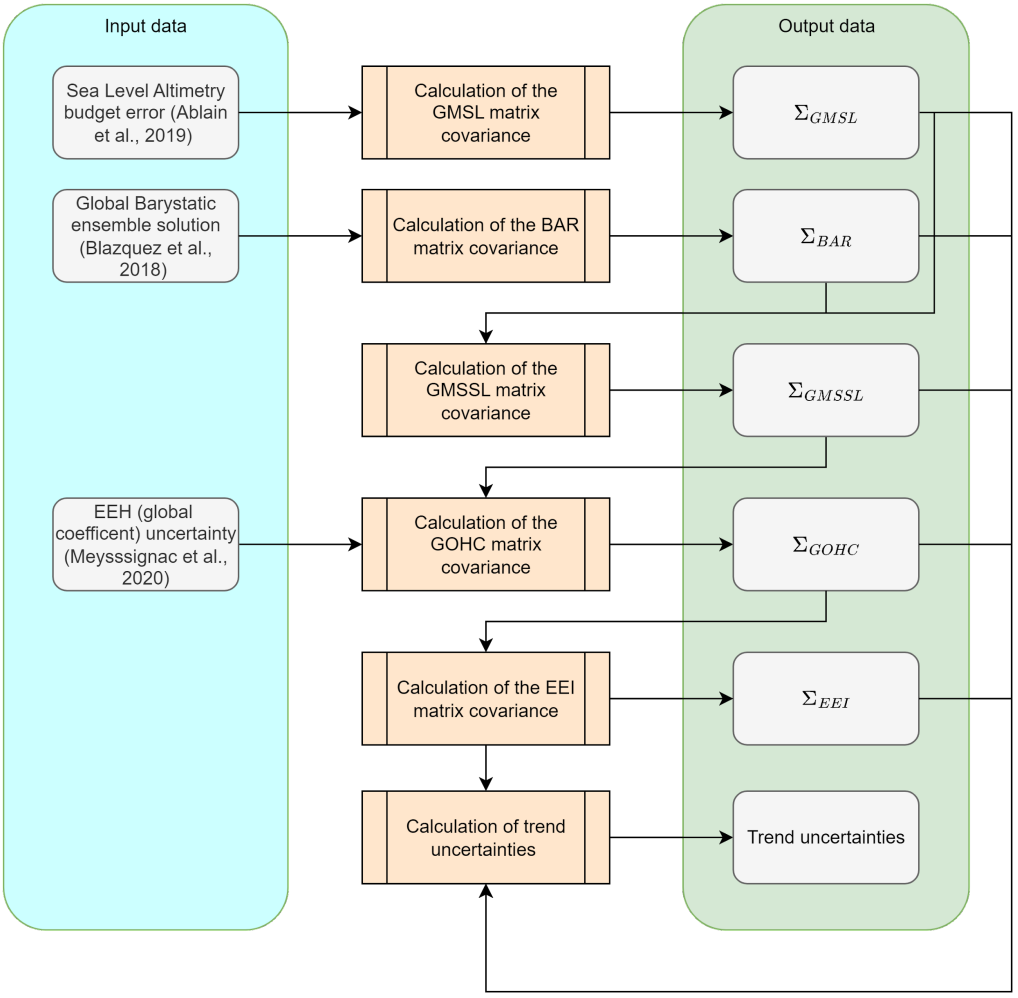

Figure 7: Uncertainty calculation and propagation chain

5.2. Input Data

The input data used are:

- the sea level altimetry error budget given by (Guérou et al., 2022) and displayed on table below,
- the ensemble of manometric sea level solutions provided by the concatenation between SLBC_cci (Horwath et al., 2022, [RD7]) and Blazquez et al. (2018) (Table 2, [RD4]).
- land mask (spatial resolution: 1° x 1°)
- the uncertainty of the global integrated expansion efficiency of heat coefficient provided by Marti et al. (2022) : $5.5.10^{-4}\, m.YJ^{-1}$

Source of errors	Error category	Uncertainty level (at 1 σ)
High frequency errors: altimeter noise, geophysical corrections, orbits ...	Correlated errors (λ = 2 months)	σ = 1.7 mm for TOPEX period σ = 1.2 mm for Jason-1 period. σ = 1.1 mm for Jason-2 period. σ = 1.0 mm for Jason-3 period.
Medium frequency errors: geophysical corrections, orbits ...	Correlated errors (λ = 1 year)	σ = 1.4 mm for TOPEX period σ = 1.2 mm for Jason-1 period. σ = 1.1 mm for Jason-2/3 period.
Large frequency errors: wet troposphere correction	Correlated errors (λ = 5 years)	σ = 1.1 mm over the period TOPEX/Jason-2 (⇔ to 0.2 mm/yr for 5 years) σ = 1.8 mm over the Jason-3 period
Large frequency errors: orbits (Gravity fields)	Correlated errors (λ = 10 years)	σ = 1.12 mm over TOPEX period (no gravimetry data on this period) σ = 0.5 mm over Jason period (⇔ to 0.05 mm/yr for 10 years)
Altimeter instabilities on TOPEX-A and TOPEX-B	Drift error	δ = 0.7 mm/yr on TOPEX-A period δ = 0.1 mm/yr on TOPEX-B period
Long-term drift errors: orbit (ITRF) and GIA	Drift error	δ = 0.12 mm/yr over 1993-2022
GMSL bias errors to link altimetry missions together	Bias errors	D = 2 mm for TP-A/TP-B D = 0.3 mm for TP-B/J1 D = 0.1mm for J1/J2 D = 0.2 mm forJ2/J3

Table 4 Altimetry GMSL error budget given at 1-sigma

5.3. Output Data

Errors are characterised with the following variance-covariance matrices:

- Σ_{GMSL},$\Sigma_{BAR}$and $\Sigma_{GMSSL}$for the global mean SL, MAN and SSL time series
- $\Sigma_{GOHC}$for the global OHC time series
- $\Sigma_{EEI}$for the EEI (for GOHC low-pass filtered at a 3 year filtering period)

5.4. Retrieval methodology

5.4.1. Calculation of the GMSL covariance matrix

5.4.1.1. Description

The objective is to calculate the error variance-covariance matrix of the GMSL time series (Σ_{GMSL}) for the time period of the study. $\Sigma_{GMSL}$is deduced from the sea level error budget described in Table 4.

5.4.1.2. Mathematical statement

We assumed that all error sources shown in Table 4 are independent from one to another. Thus the matrix is the sum of the individual variance-covariance matrices of each error source in the sea level error budget:

$$\Sigma_{GMSL} = \sum_{i=1}^{n} \Sigma_{Error_i} \qquad \text{Eq. 20}$$

Each matrix is calculated from a large number of random draws (> 1000) of simulated error signal where the correlation is modelled with a Gaussian attenuation based on the wavelength (λ) of the errors: $e^{-\frac{1}{2}(\frac{t}{\lambda})^2}$.

5.4.1.3. Comments/Limitations

This matrix is based on the current knowledge of altimetry measurement errors. As the altimetry record increases in length with new altimeter missions, the knowledge of the altimetry measurement also increases and the description of the errors improves. Consequently, the error variance-covariance matrix is expected to change and improve in the future – hopefully with a reduction of measurement uncertainty in new products.

It is also important to note that the error budget approach applied here to derive the variance-covariance matrix is conservative. In other words, sea level altimetry errors may be overestimated with respect to reality. Further studies are planned to analyse the sensitivity of this error budget on the GOHC and EEI uncertainties.

5.4.2. Calculation of the BAR covariance matrix

5.4.2.1. Description

The objective is to calculate the error variance-covariance matrix of the BAR time series (Σ_{BAR}) for the time period of the study. $\Sigma_{BAR}$is derived from a BAR ensemble deduced from the ensemble of manometric sea level solutions containing the full 120 grids datasets.

5.4.2.2. Mathematical statement

The MAN data are available worldwide. Only ocean data are kept by applying the land mask. At each time step (monthly), the global average of each manometric sea level solution grid (1x1 degree) is calculated by performing a weighted average taking into account the sea surface of each cell. The weighting grid (w) takes into consideration the surface area of each cell but also the water/land ratio.

The resulting BAR ensemble solutions contains n temporal vectors noted hereafter X_i for i=1 from 1 to n. The variance-covariance matrix (Σ_{BAR}) is the matrix whose entry is the covariance:

$$\Sigma_{BAR}(i,j) = cov(X_i, X_j) = E[(X_i - E[X_i])(X_j - E[X_j])] \quad \text{Eq. 21}$$

where E is the mean operator.

Addition of a block matrix in the variance-covariance matrix into the data gap of GRACE(-FO)

The gap-filling algorithm (described in section 4.4.3.2.) underestimated the part of the signal driven by sub-annual processes. Adding a high frequency component (section 4.4.3.2.) to the ensemble with a stochastic method allowed us to correct a part of this high frequency signal, inducing an increase of the coefficients located on the diagonal of the variance-covariance matrix (Σ_{BAR}). However, the non-diagonal terms of Σ_{BAR} characterising the time correlated errors (for example those linked with inter-annual variability) are still underestimated. In order to obtain more realistic uncertainties into the data gaps, an empirical a posteriori approach is developed, based on the following steps:

- identification of a period of the same duration as the period of the data gap
- extraction of the terms of the block variance-covariance matrix on this period
- addition of the matrix taken on the block matrix of the period to be reconstructed

BAR uncertainties based on the variance-covariance matrix are now taking into account the time correlated errors. Note that this method is just applied to the main data gap corresponding to the transition between GRACE and GRACE-FO (2017-2018).

5.4.2.3. Comments/Limitations

The new ensemble mean provided contains 120 solutions which is a important number of solutions to calculate Σ_{BAR}. However the mathematical formulation above assumes a normal distribution of the different BAR solutions. In practice, it is not fully the case. Thorough investigations must be performed to analyse the impact of this approximation.

In contrast to altimetric sea level errors, the ensemble error approach applied here to derive a variance-covariance matrix could be considered as an optimistic view of the BAR error description. This means that BAR uncertainties could be underestimated.

Concerning the extension of GRACE data with SLBC_cci data, it has been chosen to extend separately each one of the 120 solutions of GRACE in the past. The uncertainty associated with the extension method was found to be larger than the uncertainty associated with the dataset

(Horwath et al., 2022, RD7). The uncertainty associated with the dataset has therefore been neglected.

It is important to note that we use the full 120 solutions for the estimation of the uncertainties of the BAR ensemble even if it has been chosen to plot the average of only 60 solutions for the BAR sea level. This implies a decentring of the uncertainties with respect to the BAR sea level, which will be centred around the ensemble mean.

5.4.3. Calculation of the GMSSL covariance matrix

5.4.3.1. Description

The objective is to compute the variance-covariance matrix of the GMSSL errors (Σ_{GMSSL}). As GMSSL is obtained by calculating the differences between GMSL and BAR, Σ_{GMSSL} is obtained by summing the variance-covariance matrices of the errors of GMSL and BAR. Indeed, since the errors of the two data sets can be considered independent, the errors are additive.

5.4.3.2. Mathematical statement

Σ_{GMSSL} is the sum of Σ_{GMSL} and Σ_{BAR}.

5.4.3.3. Comments/Limitations

The proposed method for propagating GMSL and BAR errors does not take into account the errors of the C3S grids and GRACE data collocation method (spatially and temporally). However, these errors are assumed to be quite small.

The estimation of a subset of BAR solutions and the propagation of uncertainty to the GMSSL also implies a decentering of the uncertainties with respect to the GMSSL sea level, which will be centred around the ensemble mean.

5.4.4. Calculation of the GOHC covariance matrix

5.4.4.1. Description

The objective is to calculate the variance-covariance matrix of the GOHC errors (Σ_{GOHC}). The errors from GMSSL time series are propagated to the GOHC time series taking into account the relationship between the GOHC and GMSSL via the global expansion efficiency of heat coefficient (ε or global IEEH) and its uncertainty (e_ϵ). Σ_{GOHC} is inferred from Σ_{GMSSL} from the following relationship (see details in next subsection).

$$GOHC(t) = \frac{GMSSL\ (t) \pm e_{GMSSL}(t)}{\epsilon \pm e_\epsilon} \qquad \text{Eq. 22}$$

5.4.4.2. Mathematical statement

In case of two uncorrelated scalar variables a and b, with a respective uncertainty e_a and e_b, the error propagation division follows the ensuing relationship (Taylor, 1997, equation 3.8):

$$(e_{\frac{a}{b}})^2 = \left(\frac{1}{b}\right)^2 * \left[e_a^{\,2} + \left(e_b * \frac{a}{b}\right)^2\right] \quad \text{Eq. 23}$$

In our case:

- a= GMSSL(t) and ϵ_a is $e_{GMSSL}(t)$
- b= global IEEH (noted ϵ) and ϵ_b is given by e_ϵ
- $\frac{a}{b} = \frac{GMSSL(t)}{GEEH} = GOHC(t)$

Thus with these notations, the first equation becomes:

$$\left(e_{GOHC(t)}\right)^2 = \frac{1}{\epsilon^2} * (e_{GMSSL}(t))^2 + \left(\frac{e_\epsilon}{\epsilon}\right)^2 * (GOHC(t))^2 \quad \text{Eq. 24}$$

which can be written in matricial notation with the variance-covariance matrices Σ_{GOHC} and Σ_{GMSSL} (containing the uncertainties $e_{GOHC}^{\,2}$ and $e_{GMSSL}^{\,2}$ respectively) as follows:

$$\Sigma_{GOHC} = \frac{1}{\epsilon^2}\Sigma_{GMSSL} + \left(\frac{e_\epsilon}{\epsilon}\right)^2 GOHC * GOHC^t \quad \text{Eq. 25}$$

5.4.4.3. Comments/Limitations

The mathematical formalism proposed for the propagation of errors from the GMSSL to the GOHC shows that the errors of the GOHC depend both on the uncertainty of the value of the IEEH coefficient and on the value of the coefficient itself. When analysing the impact of changing this coefficient and its uncertainty (from Levitus et al., 2012/Kuhlbrodt and Gregory, 2012 to Marti et al. (2022), we found that this significantly reduced GOHC and EEI uncertainties.

The estimation of a subset of BAR solutions and the propagation of uncertainty to the GOHC also implies a decentering of the uncertainties with respect to the GOHC, which will be centred around the ensemble mean.

5.4.5. Calculation of the EEI covariance matrix

5.4.5.1. Description

The objective is to compute the variance-covariance matrix of errors of the EEI (Σ_{EEI}) from Σ_{GOHC}. Contrary to the error propagation for the GMSSL or the GOHC where a formal approach has been specified, an empirical approach is proposed here where a set of solutions of GOHC errors (> 1000) is generated in a random way from Σ_{GOHC}. Therefore, the set of error solutions of the corresponding EEI is computed as described in the algorithm of section 4.4.8.. Then the variance-covariance matrix of EEI is computed from this set following the algorithm described in section 5.4.2..

5.4.5.2. Mathematical statement

Each random solution of GOHC errors is a vector following a Gaussian vector of mean 0 and covariance matrix Σ_{GOHC}: $N(0, \Sigma_{GOHC})$. They are obtained by the product of the Cholesky decomposition of Σ_{GOHC} (which is semi positive-definite matrix by construction), and a random vector following (R_k) a Gaussian vector of mean 0 and covariance matrix the identity: $N(0, I)$.

Σ_{GOHC}can be written by Cholesky:

$$\Sigma_{GOHC} = AA^t \qquad \text{Eq. 26}$$

and each GOHC error vector (e_k) equals:

$$e_k = AR^t{}_k \qquad \text{Eq. 27}$$

Each e_k is then filtered by a low-pass filter (Lanczos) with cut-off period λ:

$$\widehat{e_k} = F_\lambda(e_k) \qquad \text{Eq. 28}$$

And the OHU variance-covariance matrix corresponds to the following calculation:

$$\Sigma_{OHU}(i,j) = cov(\widehat{e_{k_i}}, \widehat{e_{k_j}}) = E[(\widehat{e_{k_i}} - E[\widehat{e_{k_i}}])(\widehat{e_{k_j}} - E[\widehat{e_{k_j}}])] \quad \text{Eq. 29}$$

where E is the mean operator.

The final operation consists in applying the formulation from Eq. 17 for the division of the GOHU by the α fraction. Σ_{EEI} is obtained simply from Σ_{GOHU} neglecting any errors in α:

$$\Sigma_{EEI}(i,j) = \frac{1}{\alpha^2}\Sigma_{OHU}(i,j)\,,\ with\ \alpha = 0.91 \quad \text{Eq. 30}$$

5.4.5.3. Comments/Limitations

The estimation of a subset of BAR solutions and the propagation of uncertainty to the EEI also implies a decentering of the uncertainties with respect to the EEI, which will be centred around the ensemble mean.

5.4.6. Calculation of trend uncertainties

5.4.6.1. Description

The objective is to calculate the trend uncertainty, adjusting a polynomial of degree 1 by an ordinary least square (OLS) method taking into account the error variance-covariance matrix for the calculation of the uncertainty.

5.4.6.2. Mathematical statement

The ordinary least square (OLS) regression method is used in this study. The estimator of β with the OLS approach is noted:

$$\hat{\beta} \sim (X^t X)^{-1} X^t y \quad \text{Eq. 31}$$

where y is the vector containing the observations (e.g. GMSL, GOHC, ...) and X the vector containing the dates of the observations.

The uncertainty in the trend estimates takes into account the correlated errors of the observations (y). So, the error is integrated into the trend uncertainty estimation. Taking into account the variance-covariance matrix (Σ) , the estimator of β becomes:

$$\hat{\beta} = N(\beta, (X^t X)^{-1}(X^t \Sigma X)(X^t X)^{-1}) \quad \text{Eq. 32}$$

5.4.6.3. Comments/Limitations

The proposed approach is also applicable for any other adjusted variables. For instance, the acceleration of the time series can be calculated from the adjustment of a polynomial of degree 2 ($a_0 + a_1X + a_2X^2$) where the acceleration (a) is given by $a = 2a_2$. The uncertainty acceleration is calculated applying the same mathematical formalism described previously for the trend.